

AMCoR

Asahikawa Medical College Repository <http://amcor.asahikawa-med.ac.jp/>

Nuclear Medicine Communications (2007) 28(9):726–735.

A compartment model analysis for investigation of myocardial fatty acid metabolism in patients with hypertrophic cardiomyopathy.

Okizaki A, Shuke N, Sato J, Sasaki T, Hasebe N, Kikuchi K, Aburano T.

A compartment model analysis for investigation of the myocardial fatty acid metabolism in patients with hypertrophic cardiomyopathy.

Atsutaka Okizaki, M.D.*

Noriyuki Shuke, M.D.*

Junichi Sato, R.T.*

Tomoaki Sasaki, M.D.*

Naoyuki Hasebe, M.D.**

Kenjiro Kikuchi, M.D.**

Tamio Aburano, M.D.*

Departments of Radiology, Asahikawa Medical College, Asahikawa, Japan*

First Departments of Internal Medicine, Asahikawa Medical College, Asahikawa, Japan**

Address correspondence:

Atsutaka Okizaki, M.D.

Department of Radiology, Asahikawa Medical College

2-1-1-1 Midorigaoka-higashi, Asahikawa 078-8510, Japan.

Phone: +81-166-68-2572

Fax: +81-166-68-2579

e-mail: okizaki@asahikawa-med.ac.jp

Abstract

Objective: The purpose of this study was to investigate the myocardial fatty acid metabolism in patients with hypertrophic cardiomyopathy (HCM) from dynamic SPECT through a compartment model analysis. **Methods:** Twenty-four normal controls, 7 patients with left ventricular hypertrophy (LVH) due to essential hypertension (eHT), and 30 patients with HCM were studied. I-123 BMIPP and Tc-99m tetrofosmin SPECT were performed. All the myocardium was divided into 13 segments, and totally 390 segments of HCM were categorized into early, moderately and severely advanced HCM segments, based on these SPECT imaging. By using the myocardial and blood pool time-activity curves, BMIPP pharmacokinetics was analyzed through a 2-compartment model. We defined k_1 and k_2 as influx and outflux rate constants between blood and myocardial reversible component, k_3 as specific uptake rate constant between myocardial reversible and irreversible compartments. **Results:** The averages of k_3 in HCM were higher than in normal. In contrast, the averages of k_1/k_2 in HCM were lower than in normal, and gradually decreased with progression of HCM. There are no significant differences in these indexes between normal controls and patients with LVH due to eHT. **Conclusion:** k_3 might be a sensitive predictor for early detection of HCM, and k_1/k_2 could be a useful index to evaluate its progression. A mathematical compartment model analysis with BMIPP SPECT study might be useful not only for identification of HCM in very early stage, but also for evaluation of the progression of HCM.

Key words:

I-123 BMIPP, Compartment model analysis, hypertrophic cardiomyopathy, Dynamic SPECT, Left ventricular hyperplasia

Background

The myocardium can use several substrates including fatty acids, glucose, lactate, pyruvate, ketone bodies and amino acids for energy production [1, 2]. In particular, fatty acids are the principal source of energy for the myocardium under aerobic conditions [1, 3].

Carbon-11 labeled palmitate, which is a 16-carbon long-chain fatty acid, has been played an important role in noninvasive evaluation of myocardial fatty acid metabolism [4]. Carbon-11 labeled acetate has also been used for investigation on fatty acid metabolism [5]. However, these radiotracers are available in only a limited number of institutions because positron emission tomography scanner and cyclotron are necessary. These devices are relatively expensive and not yet widely available.

In contrast, gamma-camera imaging with single-photon radionuclides is widely available because the system is not so expensive. Several iodine 123-labeled free fatty acids and its analogs, such as iodophenylpentadecanoic acid (IPPA), 15-(p-iodophenyl)-9-(R,S)-methylpentadecanoic acid and 15-(p-iodophenyl)-3-(R,S)-methylpentadecanoic acid (BMIPP) have been widely used for the evaluation of myocardial fatty acid uptake and metabolism [6-8].

Iodine 123-labeled BMIPP (I-123 BMIPP) is a modified fatty acid in which methyl branching has been introduced into the β -position to inhibit beta-oxidation in human myocardium, and has suitable characteristics for myocardial single-photon emission computed tomography (SPECT) because of its high uptake and longer retention in the myocardium [7, 9].

I-123 BMIPP cardiac SPECT has been used in patients with various heart diseases including hypertrophic cardiomyopathy (HCM). Several authors reported the reduction of myocardial I-123 BMIPP uptake related to the myocardial abnormalities, including HCM and ischemic heart diseases [10-12]. Kawai et al. showed that the area at risk could be estimated using I-123 BMIPP imaging in patients with myocardial infarction[13], and Takeishi et al.

reported that I-123 BMIPP imaging was able to detect the presence of a coronary artery stenosis and exercise-induced myocardial ischemia, and to determine the functional severity of coronary artery disease[14]. In addition, Sasaki et al. reported that I-123 BMIPP SPECT was useful to distinguish the high risk patients with congestive heart failure [15]. Moreover, Kobayashi et al. reported that a perfusion-metabolic mismatch on I-123 BMIPP and myocardial perfusion imaging was observed more frequently in patients with HCM than with hypertension, and I-123 BMIPP imaging was useful in investigating the pathogenesis of HCM and differentiation from secondary cardiac hypertrophy[16]. Most of the literatures about human myocardial fatty acid metabolism have been based on static myocardial SPECT images including those above. Only Saito et al [17] and Kitagawa et al [18] performed an analysis of BMIPP dynamic SPECT with Rutland method. They concluded that the analysis facilitated early detection of doxorubicin-induced myocardial damage. Kondo et al [19] investigated the myocardial fatty acid metabolism using reduction rate derived from time-activity curve (TAC) and reported metabolic disorders caused by interferon therapy was detected before abnormalities in Holter electrocardiogram (ECG) or echocardiography became obvious.

A mathematical compartment model analysis is potentially useful for estimating the intracellular metabolism [20]. Sakamoto et al evaluated the fatty acid metabolism using a compartment model analysis in a Langendorff model of an isolated and perfused rabbit hearts [21], but to our knowledge, the use of a compartment model analysis for human cardiac BMIPP metabolism has not been reported previously.

In this study, we hypothesized that the abnormality of fatty acid uptake and metabolism may occur before becoming recognizable on SPECT images in patients with HCM. A mathematical compartment model analysis and dynamic SPECT data could be useful for detecting such abnormality of myocardial fatty acid metabolism. I-123 BMIPP dynamic cardiac SPECT acquisition and a mathematical compartment model analysis were performed in patients with HCM. Furthermore, results of the analysis between HCM and left ventricular hypertrophy

(LVH) due to essential hypertension (eHT) were compared, to investigate the potential partial volume effects in our study, because attenuation and scatter corrections were not performed.

Methods

Subjects

Twenty-four patients, who were suspected of having some heart disease but eventually proved to be normal through the clinical work-up, were selected as normal control subjects. Findings on ECG, echocardiography, coronary angiography and myocardial perfusion and fatty acid metabolism SPECT imaging in them were normal. These normal control subjects (17 men, 7 women; mean age, 61.4 +/- 12.5 years; range, 27-79 years), 7 patients with LVH due to eHT (5 men, 2 women; mean age, 62.0 +/- 9.15 years; range, 46-74 years), and 30 patients with HCM (19 men, 11 women; mean age, 56.3 +/- 15.3 years; range, 25-76 years) were studied. They were admitted to our hospital from January 1999 to December 2006. No patients in this study had ischemic heart disease. The 7 patients with LVH had no significant valvular disease, but had a LVH on echocardiography and a history of eHT. The diagnosis of HCM was made based on the clinical findings and ECG, and on an echocardiographic demonstration of a hypertrophied LV wall in the absence of any other cardiac or systemic disease, in accordance with recently proposed diagnostic criteria [22, 23]. All the patients and their families had given their informed consents to this study.

Radiopharmaceutical

I-123 BMIPP was obtained from Nihon Medi-Physics Co., Ltd. (Nishinomiya, Japan). Tc-99m tetrofosmin was prepared using a kit vial (Myoview®, Nihon-Medipysics, Nishinomiya, Japan) and Tc-99m pertechnetate freshly eluted from a Tc-99m generator (Mediatech®, Nihon-Medipysics, Nishinomiya, Japan). Tc-99m labeling of tetrofosmin was

performed 30 minutes before the injection.

Imaging protocol

All subjects were instructed to fast on the day of this study and to continue fasting until an acquisition was completed. A dose of 111 MBq of I-123 BMIPP was administered intravenously to subjects in a supine position. Immediately after an injection, dynamic myocardial SPECT imaging was performed using a rotating triple-headed digital gamma camera system equipped with low-energy general-purpose collimators (GCA-9300/DI, Toshiba, Tokyo, Japan). The in-plane spatial resolution of this system was 20 mm FWHM in the air. Camera rotation of 120 degrees around the chest in 30 seconds covered the projections over 360 degrees with a 64 x 64 pixel matrix, using an energy window of 10% centered at 160 KeV. The pixel size was 6.4 x 6.4 mm. A total of 20 series of projection data were acquired for 15 minutes. Static myocardial SPECT imaging was also performed approximately 20 minutes after injection. Tc-99m tetrofosmin gated SPECT was performed within 2 weeks period before or after the BMIPP SPECT study. A SPECT data acquisition was performed 2 hours after intravenous injection of 740 MBq of Tc-99m tetrofosmin, using the same camera system and collimator settings. Sixty-four projections over 360-degree were recorded in a 64 x 64 pixel matrix with an acquisition time of 25 seconds per each projection, using an energy window of 10% centered at 140 KeV. The pixel size was 6.4 x 6.4 mm. ECG-gated SPECT were performed at 8 frames per cardiac cycle, with the acceptance window set at 20%.

After these acquisitions, reconstruction was performed on a dedicated data processing unit (GMS-5500DI, Toshiba, Tokyo, Japan). Standard filtered back-projection algorithm without attenuation and scatter correction was chosen. A ramp filter was used after preprocessing with a Butterworth filter (order 8, cutoff-frequency 0.22 cycle/cm) to reconstruct transaxial images with 6.4 mm thickness. Oblique sections including short-axial slices with 1-pixel thickness were then generated by pixel reorientation. Wall motions and thickening were evaluated with the

Cedars-Sinai quantitative gated SPECT program, and echocardiography [24, 25].

Categorization of myocardial segments

The uptake of Tc-99m tetrofosmin and I-123 BMIPP are preserved in very early phase of HCM [16, 26]. In this phase, a hypertrophy is only findings on these SPECT imaging. In moderately advanced phase of HCM, the uptake of I-123 BMIPP is reduced, but the uptake of myocardial perfusion imaging agent is preserved [27]. In severely advanced phase, the uptake of myocardial perfusion imaging agent is also reduced [28]. According to these facts, we defined early HCM as normal uptake of Tc-99m tetrofosmin and I-123 BMIPP, moderately advanced HCM as normal uptake of Tc-99m tetrofosmin and decreased uptake of I-123 BMIPP, and severely advanced HCM as decreased uptake of Tc-99m tetrofosmin and I-123 BMIPP.

The myocardium was divided into 13 segments, like the recommendations of the American Heart Association standard myocardial segmentation [29]. According to the result of myocardial perfusion SPECT imaging with Tc-99m tetrofosmin and fatty acid metabolism SPECT imaging with I-123 BMIPP, which visually interpreted by 2 nuclear medicine physicians, the segments of the patients with HCM categorized into early, moderately advanced and severely advanced segments.

Finally, a total of 793 segments were studied in this study, including 312 normal segments, 91 LVH due to eHT segments, 314 early HCM segments, 59 moderately advanced HCM segments and 17 severely advanced HCM segments.

A rectangular region of interest (ROI) was placed manually on vertical long-axis image in the center of the LA for measurement of input function. A ROI of myocardium (Apical segment) was placed on the vertical long-axis image and 12 ROIs of myocardium (except for the Apical segment) were also placed in each segment on short-axis images. The size of these ROIs were 12.8 x 12.8 mm. Input function and tissue TACs were generated from the serial images.

Compartment model analysis

A mathematical compartment model analysis was performed to obtain information about the tracer kinetics.

Our 1- and 2-compartment models were shown in Figure 1A and 1B. This 1-compartment model was composed of blood compartment and reversible tissue compartment (C1). Mathematically this model can be expressed as:

$$dC1(t)/dt = k1B(t) - k2C1(t)$$

$$C1(t) = k1e^{-k2t} \int_0^t B(t) e^{k2t} dt$$

$$C1(0) = 0$$

where $C1(t)$ = I-123 BMIPP amount in the reversible tissue compartment; $B(t)$ = I-123 BMIPP amount in the blood; $k1$ = influx rate constant for the reversible tissue compartment (1/second); $k2$ = outflux rate constant for the reversible tissue compartment (1/second). $k1$ and $k2$ were set to be adjustable.

In 2-compartment model, irreversible tissue compartment (C2) was added to the 1-compartment model. Mathematically this model can be expressed as:

$$C1(t) = k1 \int_0^t B(\tau) \cdot e^{-(k2+k3)(t-\tau)} d\tau$$

$$C2(t) = k3 \int_0^t C1(t) dt$$

$$C(t) = C1(t) + C2(t)$$

$$= \frac{k2}{k2+k3} C1(t) + \frac{k1 \cdot k3}{k2+k3} \int_0^t B(\tau) d\tau$$

$$C1(0) = 0$$

$$C2(0) = 0$$

where $C1(t)$ = I-123 BMIPP amount in the reversible tissue compartment; $C2(t)$ = I-123 BMIPP amount in the irreversible tissue compartment; $C(t)$ = myocardial counts; $B(t)$ = I-123 BMIPP amount in the blood; $k1$ = influx rate constant for the reversible tissue compartment (1/second); $k2$ = outflux rate constant for the reversible tissue compartment (1/second); $k3$ = specific uptake rate constant for the irreversible compartment (1/second). $k1$, $k2$ and $k3$ were set to be adjustable in this model.

Myocardial tissue TACs were fitted to $C1$ or C depends on the model, using blood pool TAC generated from ROI placed in the center of left atrium (LA) as input function.

In the first step, to estimate the validity of these models, we performed TAC fitting by the least squares method and calculated each parameter using WinSAAM software version 3.0.1 (National Institutes of Health, Bethesda, Maryland, USA). Based on these results, a statistical evaluation was performed to decide which model was better.

Second, we employed the more proper model and calculated each rate constant to estimate quantitative information about BMIPP metabolism in the myocardium. This procedure was performed automatically by using an in-house written software program, which was written in Visual Basic version 6.0 (Microsoft, Redmond, Washington, USA), on a personal computer (Dell Precision 360 Workstation; Dell Computer, Round Rock, Texas, USA) with Microsoft Windows XP operating system (Microsoft, Redmond, Washington, USA). The software algorithm was composed of 2 essential components, namely, generation of TAC data from dynamic images, and estimation of the model parameters by nonlinear fitting of the TAC data. Damping Gauss-Newton method as a weighted nonlinear least squares regression method was selected to estimate each model parameter. The data were weighted using fractional standard deviations (FSDs) assumed to be 10% of the data. When the improvement in sum of square becomes 0.1% or less by further iteration, the fitting calculation was judged to be converged.

Additionally, k_1/k_2 , k_1k_3/k_2 (1/second) and $k_1k_3/(k_2+k_3)$ (1/second) were calculated. k_1/k_2 represents the distribution volume (Vd) of C1, k_1k_3/k_2 represents the influx into C2, and $k_1k_3/(k_2+k_3)$ denotes a clearance of I-123 BMIPP from blood corresponding to the tissue clearance obtained by the Patlak plot. All these indexes were evaluated and compared in normal, early, moderately advanced and severely advanced HCM ROIs. Furthermore, to investigate the potential partial volume effects in our study, these indexes were also compared in normal and LVH due to eHT.

Statistical analysis

The Akaike information criterion (AIC) was used to evaluate the validity of 1- and 2-compartment models [30]. The equation was as follows,

$$AIC = n \ln (RSS) + 2p$$

where p is the number of parameters in the model, n is the number of data points and RSS is the residual sum of squares. It can be seen that small AIC scores should be preferred.

To test the between-group differences, the 2-tailed Student t test or Welch modified t test was used depending on the equality of variances which calculated by using Levene's test. Pearson product-moment correlation coefficient was used to investigate the deviation of fitted curve from each data. Binominal and multinominal logistic regression analyses were performed to evaluate which parameter could be better predictor for HCM. A P value less than 0.05 was considered statistically significant.

Results

SPECT imaging

Dynamic SPECT acquisitions were successfully completed in all patients. Figure 2 shows an example of SPECT image. The wall motion and thickening were normal on QGS and

echocardiography in all of them.

Model evaluation

1- and 2-compartment model analyses for 39 randomly selected ROIs (13 each from normal, early and severely advanced HCM segments) were performed, to determine which model was better. In this procedure, all parameters were converged to certain finite values with WinSAAM software.

AIC scores from the 1- and 2-compartment models are compared in the bar graph of Figure 3. The average AIC scores of 1-compartment model analysis, which calculated in normal, early, moderately advanced and severely advanced HCM ROIs, were 111.5 +/- 4.96, 110.4 +/- 3.82, 108.5 +/- 4.09 and 108.6 +/- 7.26, respectively. On the other hand, the average AIC scores of 2-compartment model analysis were 98.1 +/- 17.6, 100.6 +/- 8.37, 99.4 +/- 8.13 and 101.9 +/- 7.14, respectively. The average AIC score of 2-compartment model in these 4 groups were small compared with those of 1-compartment model. Furthermore, there were statistically significant differences. The P value between 1- and 2-compartment model analyses in normal and moderately advanced HCM ROIs were less than 0.01, in early and severely advanced HCM ROIs were less than 0.0005.

These results indicated 2-compartment model was better than 1-compartment model in our study.

Compartment model analysis

According to the results of model evaluation, 2-compartment model analysis was adopted for all ROIs. All parameters were converged to certain finite values using our in-house written software program.

Figure 4A shows a typical TAC of input function. Graphs also show typical time-activity data in normal, early, moderately advanced and severely advanced HCM ROIs (Figure 4B-E,

respectively). Superimposed are the fitted curves derived from the 2-compartment model analysis.

Pearson product-moment correlation coefficients were calculated to evaluate the validity of curve fittings. The average values in normal, early, moderately advanced and severely advanced HCM groups were 0.89 +/- 0.11, 0.87 +/- 0.10, 0.85 +/- 0.11 and 0.82 +/- 0.12 (P < 0.01 in all groups), respectively.

Results of 2-compartment model analysis are summarized in Table 1. The average of FSDs derived from normal, LHV, early, moderately advanced and severely advanced HCM groups were as follows: normal groups, [k1, k2, k3] = [149.2% +/- 150.1%, 169.9% +/- 159.1%, 32.7% +/- 12.9%]; LVH groups, [k1, k2, k3] = [169.6% +/- 165.7%, 192.5% +/- 173.9%, 34.2% +/- 11.1%]; early HCM groups, [k1, k2, k3] = [180.9% +/- 201.6%, 207.4% +/- 210.3%, 38.1% +/- 31.5%]; moderately advanced HCM groups, [k1, k2, k3] = [114.6% +/- 102.4%, 137.0% +/- 109.8%, 33.7% +/- 13.8%]; severely advanced HCM groups, [k1, k2, k3] = [280.3% +/- 456.2%, 310.1% +/- 484.5%, 32.6% +/- 10.5%], respectively. According to these results, FSDs of k1 and k2 were greater than 100% in normal, LVH, early, moderately advanced and severely advanced HCM groups, but that of k3 was less than 40%. Results of a typical correlation matrix for data fitted to the 2-compartment model are as follows,

$$\begin{bmatrix} 1 & -0.996 & 0.261 \\ -0.996 & 1 & -0.293 \\ 0.261 & -0.293 & 1 \end{bmatrix}$$

Here the components of the matrix p_{ij} are the correlation coefficients for parameter i and j , where parameter 1 is k_1 , 2 is k_2 and 3 is k_3 . It is seen that there is high correlation between k_1 and k_2 (-0.996). This tendency was seen in all data sets. However, an error of k_1/k_2 , which estimated with the error propagation rule, was very small. For example, in this case, the error of

k_1/k_2 was only 1.67%. Standard deviations (SDs) of k_1/k_2 , k_1k_3/k_2 , $k_1k_3/(k_2+k_3)$ were not so large in these 5 groups (Table 1). From these results, k_1 and k_2 were omitted from individual comparison because of their large errors of estimates, other parameters were used for further analysis.

The averages of k_3 in all HCM groups were significantly higher than in normal ($P < 0.00001$ in early and moderately advanced HCM groups, $P < 0.05$ in severely advanced HCM group). In contrast, the averages of k_1/k_2 in all HCM groups were significantly lower than in normal ($P < 0.00001$ in early and moderately advanced HCM groups, $P < 0.005$ in severely advanced HCM group), and k_1/k_2 gradually decreased with progression of HCM. The average of k_1k_3/k_2 in severely advanced HCM group was significantly lower than normal ($P < 0.05$). The averages of $k_1k_3/(k_2+k_3)$ in moderately advanced HCM groups were lower than normal ($P < 0.05$) and it in severely advanced HCM group was lower than in the other groups ($P < 0.005$).

In comparison with the normal and LVH due to eHT group, there were no statistically significant differences in these indexes (Table 1). The average values of pearson product-moment correlation coefficients in LVH due to eHT group was 0.87 ± 0.10 ($P < 0.01$).

Additionally, the statistically significant correlation factor was estimated by using binominal (non-HCM or HCM) and multinomial (early HCM, moderately or severely advanced HCM) logistic regression analyses (Table 2A and 2B). The significant correlation factors with binomial logistic regression analysis were k_3 ($P < 0.001$), $k_1k_3/(k_2+k_3)$ ($P < 0.001$) and k_1k_3/k_2 ($P < 0.005$), and with multinomial logistic regression analysis were k_3 ($P < 0.05$) and k_1/k_2 ($P < 0.01$).

Discussion

Generally speaking, complicated compartment model has many parameters, and tends to fail for parameter estimation. Considering mechanism of fatty acid metabolism in myocardium,

more complex model might be ideally suitable for investigation of fatty acid metabolism [21], whereas clinical data include noise and artifacts. For this reason, we selected simple but clinically sufficient models to obtain each rate constant.

The first compartment was defined as reversible myocardial compartment and second compartment was defined as irreversible myocardial compartment in this study (Figure 1A and 1B). BMIPP has a long retention in the myocardium by incorporation into the triglyceride (TG) pool in early phase [31]. Based on our 2-compartment model, temporal change of the counts in each compartment at approximately 20 minutes after injection of I-123 BMIPP was simulated with Win SAAM software (Figure 5). The percentage of myocardial counts in C1 and C2 were 16.2% and 83.8%. Hosokawa et al. reported that the percentage of TG pool in canine myocardium was 84.4% at 30 minutes after BMIPP injection [32]. Compared our model simulation to Hosokawa's study, reversible (C1) and irreversible (C2) compartments might represent cytoplasm and TG pool in our 2-compartment model, because the percentage of counts in C2 was greater than 80% at 20 minutes after I-123 BMIPP injection and similar to it in TG pool in the previous paper.

In our study, k_3 in HCM were higher than normal. On the other hand, k_1/k_2 (V_d of C1) was decreased with the progression of HCM. These results suggested a fatty acid shifted from cytoplasm to TG pool in HCM even if the disease was very early phase and no apparent change was observed with visual interpretation by nuclear medicine physicians. The degree of BMIPP uptake closely reflected the myocardial ATP concentration, and mitochondrial functions [33, 34]. Therefore, in damaged myocardium in patients with progressed HCM, the cause of reduction of BMIPP uptake is considered to be the impaired mitochondrial function with limited ATP generation. In deed, subtle structural changes of mitochondria in myocardium of cardiomyopathic hamster were observed with electron microscopy [35]. When mitochondrial function reduced, the concentration of fatty acid in the myocardium might be increased. High concentration of fatty acid induced arrhythmia and myocardial hypokinesia [36-38]. Actually,

TG pool was reactively enlarged under high concentration of fatty acid in myocardium to absorb the excess fatty acid and avoid the cardiotoxicity [39], and TG accumulation was increased in damaged myocardium [40]. Considering these reports, the increase of k_3 in the HCM groups was probably related to mitochondrial dysfunction, and these subtle changes in very early phase could be detected by mathematical compartment analysis.

The averages of k_1k_3/k_2 were not decreased in early and moderately advanced HCM. The reason of this result was considered as follows: In relatively early HCM, increasing of k_3 was counteracted by decreasing of k_1/k_2 . But in severely advanced HCM, the decreasing of k_1/k_2 might be larger than the increasing of k_3 . $k_1k_3/(k_2+k_3)$, which represents a I-123 BMIPP tissue clearance obtained by the Patlak plot, were decreased in moderately and severely advanced HCM, but there was no statistically significant difference between in normal and in early HCM. This result indicated that it was difficult to discriminate early HCM from normal by visual approach or quantitative approach with Patlak plot. In consideration of these results, a mathematical compartment model analysis might be useful for an earlier detection of HCM.

Hypertrophy of myocardium is frequently seen in patients with HCM. When the thicknesses of myocardium are different, partial volume effect should be corrected to evaluate the uptake without bias. When the myocardial hypertrophy is obvious, the bias probably increases the V_d of C_1 . But according to our results, the k_1/k_2 , which represents V_d of C_1 , in all HCM groups were lower compared with that in normal. This result suggested that the reduction of V_d in patients with HCM was significant even if the bias affected the results of this study. Moreover, there were no significant differences in all indexes between normal and LVH due to eHT group.

Limitation

This study has several limitations that should be mentioned. First, attenuation and scatter corrections were not performed in reconstruction of SPECT images. This could influence the

TAC, especially in ROIs of inferior wall. Second, the time resolution for the dynamic SPECT acquisition might not be enough to determine the k_1 and k_2 precisely. But, as mentioned above, at least k_3 and k_1/k_2 might be reliable indexes.

Conclusion

The present study demonstrated that k_3 might be sensitive predictor for early detection of HCM, and k_1/k_2 could be useful index to evaluate the progression of HCM. However, uptake of I-123 BMIPP was not reduced in early HCM group at least with visual qualitative approach. These results indicated that a mathematical compartment model analysis might be useful to detect subtle change of fatty acid metabolism in patients with HCM, and not only for identification of HCM in very early stage, but also for evaluation of the progression of HCM.

References

1. Neely JR, Rovetto MJ, Oram JF. Myocardial utilization of carbohydrate and lipids. *Prog Cardiovasc Dis.* 1972;15:289-329.
2. Bing RJ. Cardiac Metabolism. *Physiol Rev.* 1965;45:171-213.
3. Opie LH. Metabolism of the heart in health and disease. I. *Am Heart J.* 1968;76:685-698.
4. Sobel BE, Weiss ES, Welch MJ, Siegel BA, Ter-Pogossian MM. Detection of remote myocardial infarction in patients with positron emission transaxial tomography and intravenous ¹¹C-palmitate. *Circulation.* 1977;55:853-857.
5. Tadamura E, Tamaki N, Matsumori A, Magata Y, Yonekura Y, Nohara R, et al. Myocardial metabolic changes in hypertrophic cardiomyopathy. *J Nucl Med.* 1996;37:572-577.
6. Fujiwara S, Takeishi Y, Tojo T, Yamaoka M, Nitobe J, Takahashi K, et al. Fatty acid imaging with ¹²³I-15-(p-iodophenyl)-9-R,S-methylpentadecanoic acid in acute coronary syndrome. *J Nucl Med.* 1999;40:1999-2006.
7. Knapp FF, Jr., Ambrose KR, Goodman MM. New radioiodinated methyl-branched fatty acids for cardiac studies. *Eur J Nucl Med.* 1986;12 Suppl:S39-44.
8. Tamaki N, Fujibayashi Y, Magata Y, Yonekura Y, Konishi J. Radionuclide assessment of myocardial fatty acid metabolism by PET and SPECT. *J Nucl Cardiol.* 1995;2:256-266.
9. Goodman MM, Kirsch G, Knapp FF, Jr. Synthesis and evaluation of radioiodinated terminal p-iodophenyl-substituted alpha- and beta-methyl-branched fatty acids. *J Med Chem.* 1984;27:390-397.
10. Tadamura E, Kudoh T, Hattori N, Inubushi M, Magata Y, Konishi J, et al. Impairment of BMIPP uptake precedes abnormalities in oxygen and glucose metabolism in hypertrophic cardiomyopathy. *J Nucl Med.* 1998;39:390-396.
11. Ohtsuki K, Sugihara H, Ito K, Matsumoto K, Taniguchi Y, Terada K, et al. [The characteristic feature of myocardial imaging with ¹²³I-labeled

- 15-(p-iodophenyl)-3R,S-methylpentadecanoic acid in hypertrophic cardiomyopathy with asymmetric septal hypertrophy]. *Kaku Igaku*.1995;32:377-385.
12. Kurata C, Tawarahara K, Taguchi T, Aoshima S, Kobayashi A, Yamazaki N, et al. Myocardial emission computed tomography with iodine-123-labeled beta-methyl-branched fatty acid in patients with hypertrophic cardiomyopathy. *J Nucl Med*.1992;33:6-13.
13. Kawai Y, Tsukamoto E, Nozaki Y, Kishino K, Kohya T, Tamaki N. Use of 123I-BMIPP single-photon emission tomography to estimate areas at risk following successful revascularization in patients with acute myocardial infarction. *Eur J Nucl Med*.1998;25:1390-1395.
14. Takeishi Y, Sukekawa H, Saito H, Nishimura S, Shibu T, Sasaki Y, et al. Clinical significance of decreased myocardial uptake of 123I-BMIPP in patients with stable effort angina pectoris. *Nucl Med Commun*.1995;16:1002-1008.
15. Sasaki R, Mitani I, Usui T, Kitamura Y, Yoshii Y, Ishikawa T, et al. Clinical value of iodine-123 beta-methyliodophenyl pentadecanoic acid (BMIPP) myocardial single photon emission computed tomography for predicting cardiac death among patients with chronic heart failure. *Circ J*.2003;67:918-924.
16. Kobayashi H, Nakata T, Han S, Takahashi N, Hashimoto A, Tsuchihashi K, et al. [Fatty acid metabolic and perfusion abnormalities in hypertrophied myocardium assessed by dual tracer tomography using thallium-201 and iodine-123-beta-methylpentadecanoic acid]. *J Cardiol*.1994;24:35-43.
17. Saito K, Takeda K, Okamoto S, Okamoto R, Makino K, Tameda Y, et al. Detection of doxorubicin cardiotoxicity by using iodine-123 BMIPP early dynamic SPECT: quantitative evaluation of early abnormality of fatty acid metabolism with the Rutland method. *J Nucl Cardiol*.2000;7:553-561.
18. Kitagawa K, Takeda K, Saito K, Okamoto S, Makino K, Maeda H, et al. Differences in fatty

- acid metabolic disorder between ischemic myocardium and doxorubicin-induced myocardial damage: assessment using BMIPP dynamic SPECT with analysis by the Rutland method. *J Nucl Med.*2002;43:1286-1294.
19. Kondo Y, Yukinaka M, Nomura M, Nakaya Y, Ito S. Early diagnosis of interferon-induced myocardial disorder in patients with chronic hepatitis C: evaluation by myocardial imaging with 123I-BMIPP. *J Gastroenterol.*2000;35:127-135.
20. Dubois F, Depresseux JC, Bontemps L, Demaison L, Keriel C, Mathieu JP, et al. Mathematical model of the metabolism of 123I-16-iodo-9-hexadecenoic acid in an isolated rat heart. Validation by comparison with experimental measurements. *Eur J Nucl Med.*1986;11:453-458.
21. Sakamoto T, Aoki M, Imai Y, Nemoto S. Carnitine affects fatty acid metabolism after cardioplegic arrest in neonatal rabbit hearts. *Ann Thorac Surg.*2001;71:648-653.
22. Richardson P, McKenna W, Bristow M, Maisch B, Mautner B, O'Connell J, et al. Report of the 1995 World Health Organization/International Society and Federation of Cardiology Task Force on the Definition and Classification of cardiomyopathies. *Circulation.*1996;93:841-842.
23. McKenna WJ, Spirito P, Desnos M, Dubourg O, Komajda M. Experience from clinical genetics in hypertrophic cardiomyopathy: proposal for new diagnostic criteria in adult members of affected families. *Heart.*1997;77:130-132.
24. Adachi I, Morita K, Imran MB, Konno M, Mochizuki T, Kubo N, et al. Heterogeneity of myocardial wall motion and thickening in the left ventricle evaluated with quantitative gated SPECT. *J Nucl Cardiol.*2000;7:296-300.
25. Germano G, Kiat H, Kavanagh PB, Moriel M, Mazzanti M, Su HT, et al. Automatic quantification of ejection fraction from gated myocardial perfusion SPECT. *J Nucl Med.*1995;36:2138-2147.
26. Narita M, Kurihara T. Is I-123-beta-methyl-p-iodophenyl-methylpentadecanoic acid imaging

- useful to evaluate asymptomatic patients with hypertrophic cardiomyopathy? I-123 BMIPP imaging to evaluate asymptomatic hypertrophic cardiomyopathy. *Int J Cardiovasc Imaging*.2003;19:499-510.
27. Ohtsuki K, Sugihara H, Umamoto I, Nakamura T, Nakagawa T, Nakagawa M. Clinical evaluation of hypertrophic cardiomyopathy by myocardial scintigraphy using 123I-labelled 15-(p-iodophenyl)-3-R, S-methylpentadecanoic acid (123I-BMIPP). *Nucl Med Commun*.1994;15:441-447.
28. Mori T, Yamabe H, Yokota Y, Fukuzaki H. Clinical significance of dipyridamole TI-201 emission computed tomography perfusion abnormality for evaluating pathophysiological and pathological aspects in hypertrophic cardiomyopathy. *Jpn Circ J*.1988;52:111-118.
29. Cerqueira MD, Weissman NJ, Dilsizian V, Jacobs AK, Kaul S, Laskey WK, et al. Standardized myocardial segmentation and nomenclature for tomographic imaging of the heart: a statement for healthcare professionals from the Cardiac Imaging Committee of the Council on Clinical Cardiology of the American Heart Association. *Circulation*.2002;105:539-542.
30. Akaike H. Information theory and an extension of the maximum likelihood principle, 2nd International Symposium on Information Theory. *Akadimiai Kiado, Budapest*.1973;267-281.
31. Fujibayashi Y, Nohara R, Hosokawa R, Okuda K, Yonekura Y, Tamaki N, et al. Metabolism and kinetics of iodine-123-BMIPP in canine myocardium. *J Nucl Med*.1996;37:757-761.
32. Hosokawa R, Nohara R, Fujibayashi Y, Okuda K, Ogino M, Hirai T, et al. Myocardial metabolism of 123I-BMIPP in a canine model with ischemia: implications of perfusion-metabolism mismatch on SPECT images in patients with ischemic heart disease. *J Nucl Med*.1999;40:471-478.

33. Ogata M. [Myocardial uptake of 125I-BMIPP in rats treated with adriamycin]. *Kaku Igaku*.1989;26:69-76.
34. Fujibayashi Y, Yonekura Y, Takemura Y, Wada K, Matsumoto K, Tamaki N, et al. Myocardial accumulation of iodinated beta-methyl-branched fatty acid analogue, iodine-125-15-(p-iodophenyl)-3-(R,S)methylpentadecanoic acid (BMIPP), in relation to ATP concentration. *J Nucl Med*.1990;31:1818-1822.
35. Thet Thet L, Takeda T, Wu J, Tsuchiya Y, Itai Y. Abnormal retention of 99mTc-TF in a hamster model of cardiomyopathy analyzed by 99mTc-TF and 125I-BMIPP autoradiography. *Ann Nucl Med*.2004;18:195-202.
36. Oliver MF, Kurien VA, Greenwood TW. Relation between serum-free-fatty acids and arrhythmias and death after acute myocardial infarction. *Lancet*.1968;1:710-714.
37. Corr PB, Gross RW, Sobel BE. Amphipathic metabolites and membrane dysfunction in ischemic myocardium. *Circ Res*.1984;55:135-154.
38. Katz AM, Messineo FC. Lipid-membrane interactions and the pathogenesis of ischemic damage in the myocardium. *Circ Res*.1981;48:1-16.
39. Lopaschuk GD, Belke DD, Gamble J, Itoi T, Schonekess BO. Regulation of fatty acid oxidation in the mammalian heart in health and disease. *Biochim Biophys Acta*.1994;1213:263-276.
40. Straeter-Knowlen IM, Evanochko WT, den Hollander JA, Wolkowicz PE, Balschi JA, Caulfield JB, et al. 1H NMR spectroscopic imaging of myocardial triglycerides in excised dog hearts subjected to 24 hours of coronary occlusion. *Circulation*.1996;93:1464-1470.

Legends

Figure 1

This schema shows the 1-compartment model (A) and the 2-compartment model (B). In 1-compartment mode, first compartment (C1) is reversible tissue compartment, k_1 and k_2 represent influx and outflux rate constant for the reversible tissue compartment, respectively. The 2-compartment model had second compartment (C2) in addition to the 1-compartment model. C1 is reversible tissue compartment and C2 is irreversible tissue compartment. k_1 and k_2 also represent influx and outflux rate constant for the reversible tissue compartment, and k_3 represents specific uptake rate constant for the irreversible tissue compartment, respectively.

Figure 2

This is an example of I-123 BMIPP dynamic SPECT images. Each image is mid-ventricular short-axis image of the same slice location. Assigned number is the frame number, the frame time is 30 seconds.

Figure 3

This bar graph shows the average AIC scores of 1- and 2-compartment model in normal, early, moderately advanced and severely advanced HCM ROIs. Data are reported as mean +/- standard deviation. The average AIC scores of 2-compartment model were significantly smaller than 1-compartment model in 4 groups of ROIs. Normal-1 and Normal-2 = 1- and 2-compartment model in normal ROIs; HCM1-1 and HCM1-2 = 1- and 2-compartment model in early HCM ROIs; HCM2-1 and HCM2-2 = 1- and 2-compartment model in moderately advanced HCM ROIs; HCM3-1 and HCM3-2 = 1- and 2-compartment model in severely advanced HCM ROIs, respectively.

Figure 4

This plot shows a typical input function (A) and fitting curves of a normal (B), an early HCM (C), a moderately advanced (D) and a severely advanced HCM ROI (E). The vertical axis shows the radioactivities (counts per 30 seconds) of the ROI in the center of the LA (A) or the segment (B-E), and the horizontal axis shows time from the injection.

Figure 5

This plot shows a simulation of each compartment with Win SAAM software. Triangles show observed data. A thin line represents the activity in the reversible tissue component (C1) and thick line represents in the irreversible tissue component (C2). The activity in reversible tissue component was gradually decreased and it in irreversible tissue component was increased with time until 15 minutes after the injection

Figure 1A

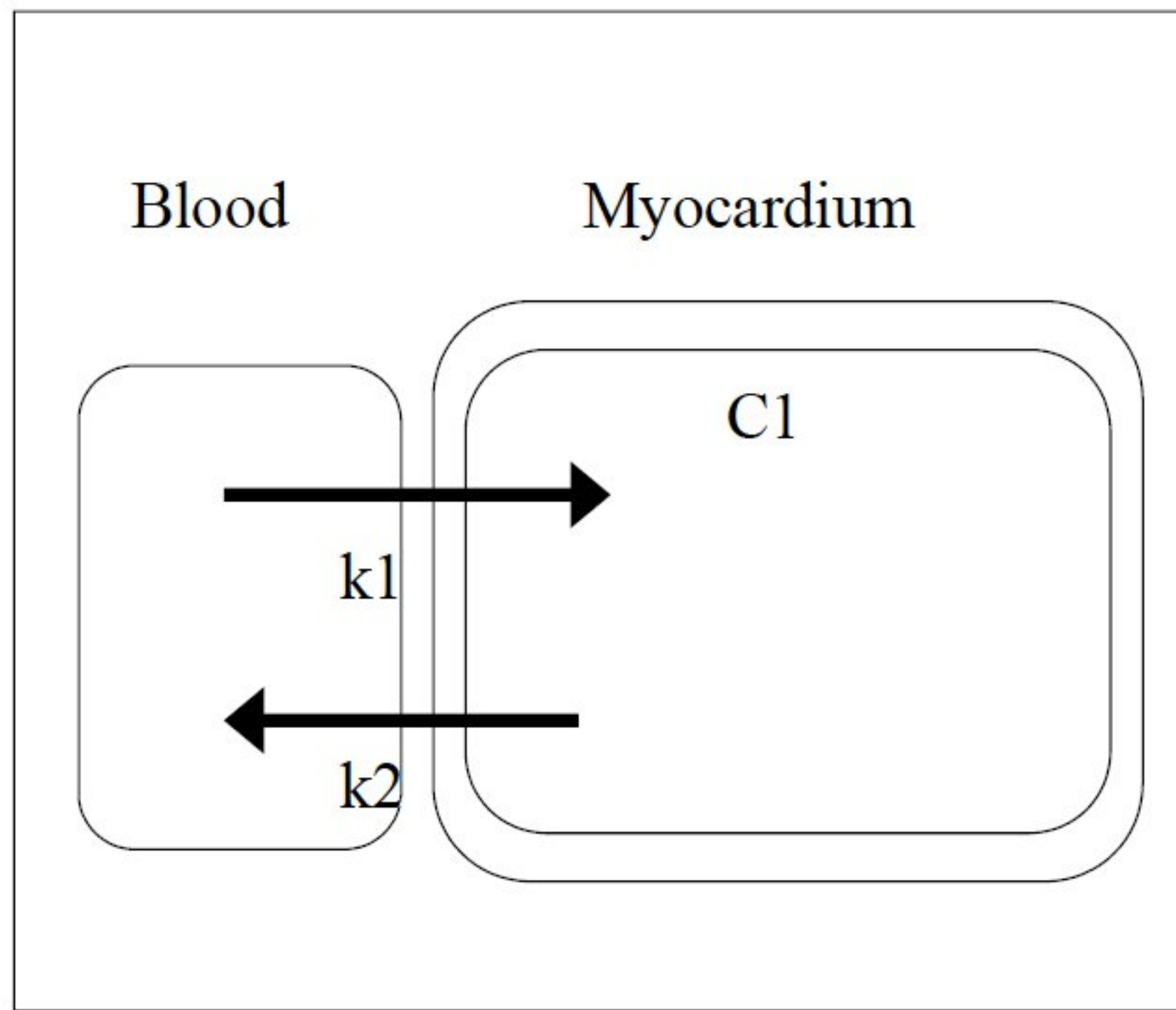


Figure 1B

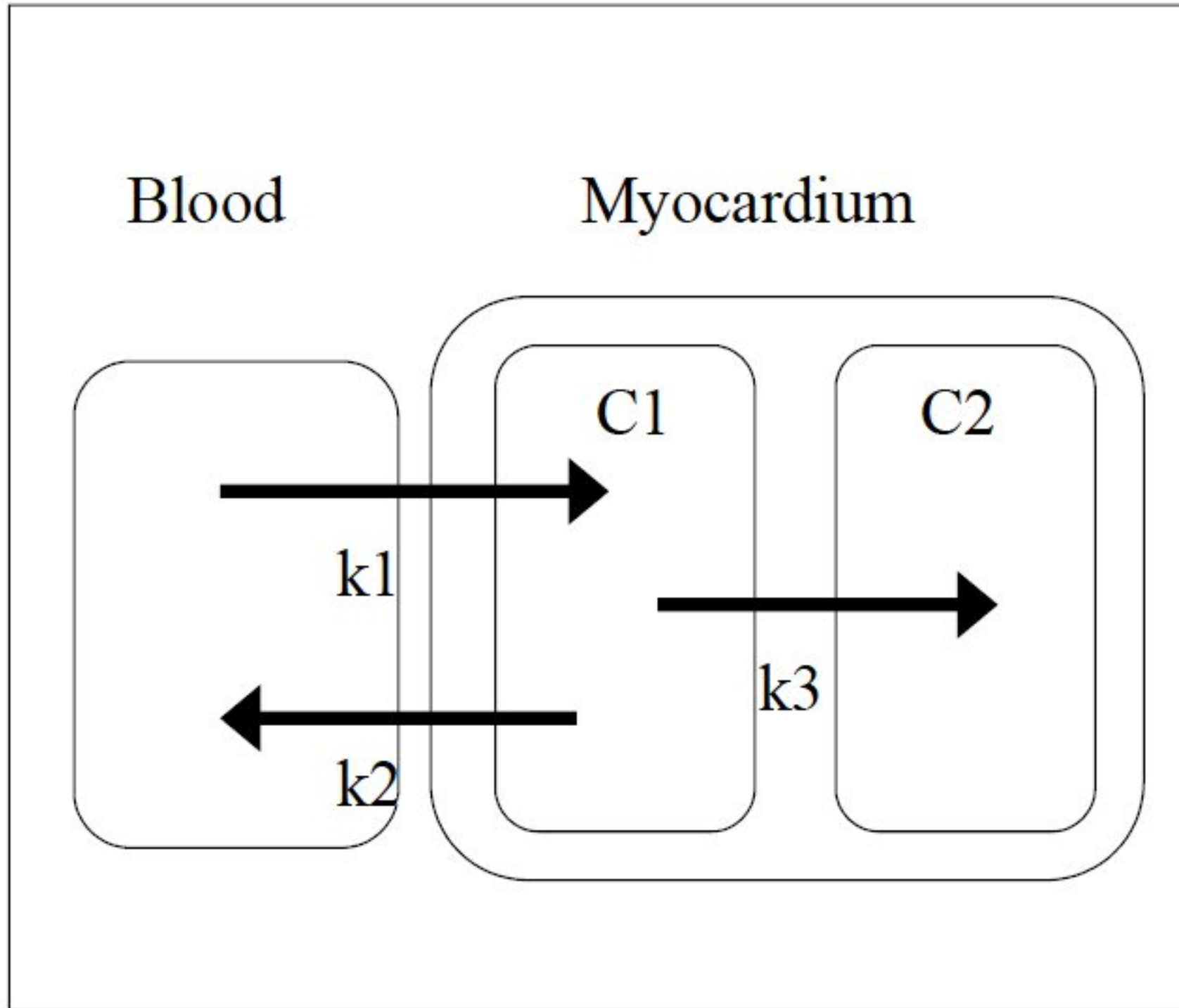


Figure 2

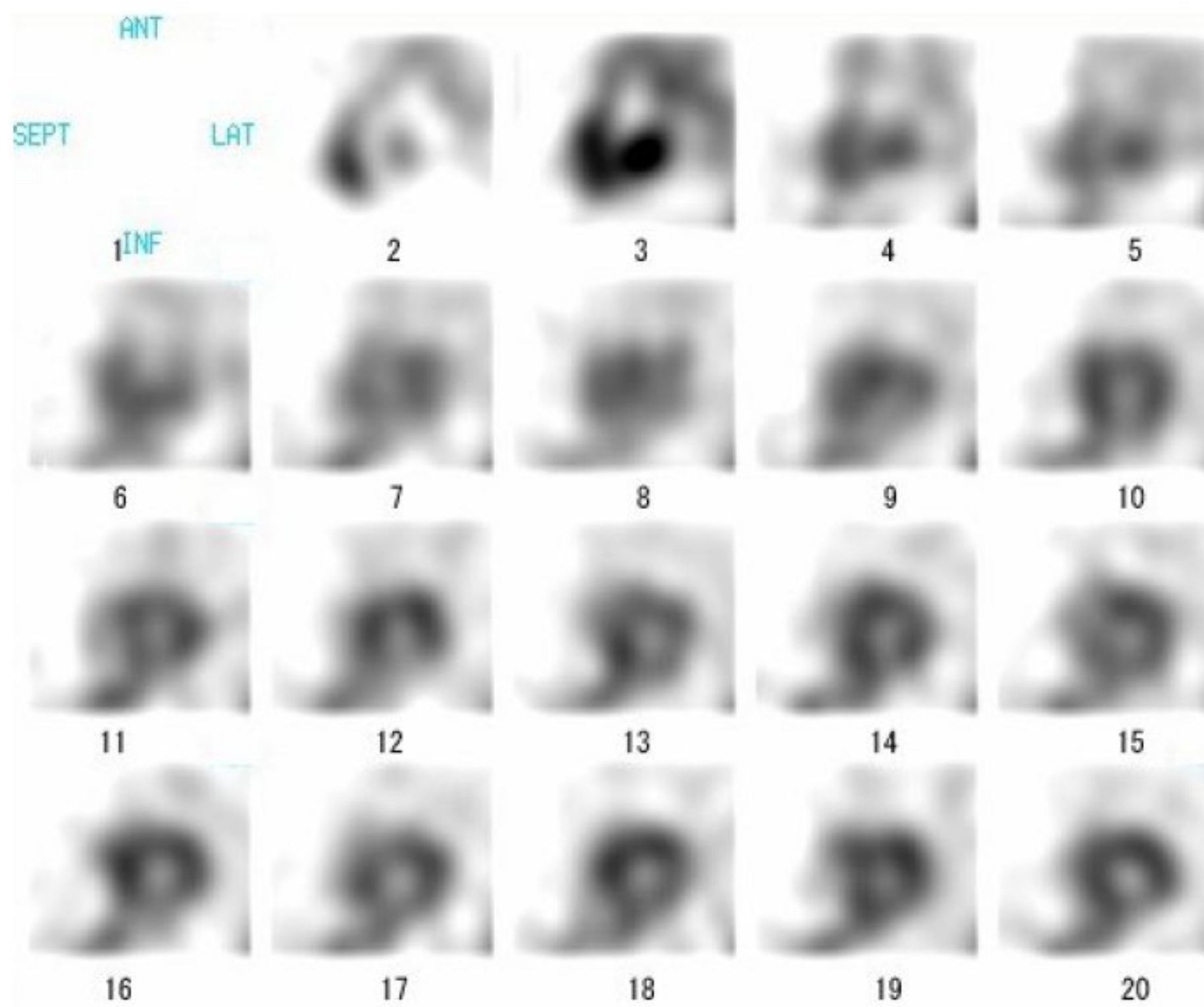


Figure 3

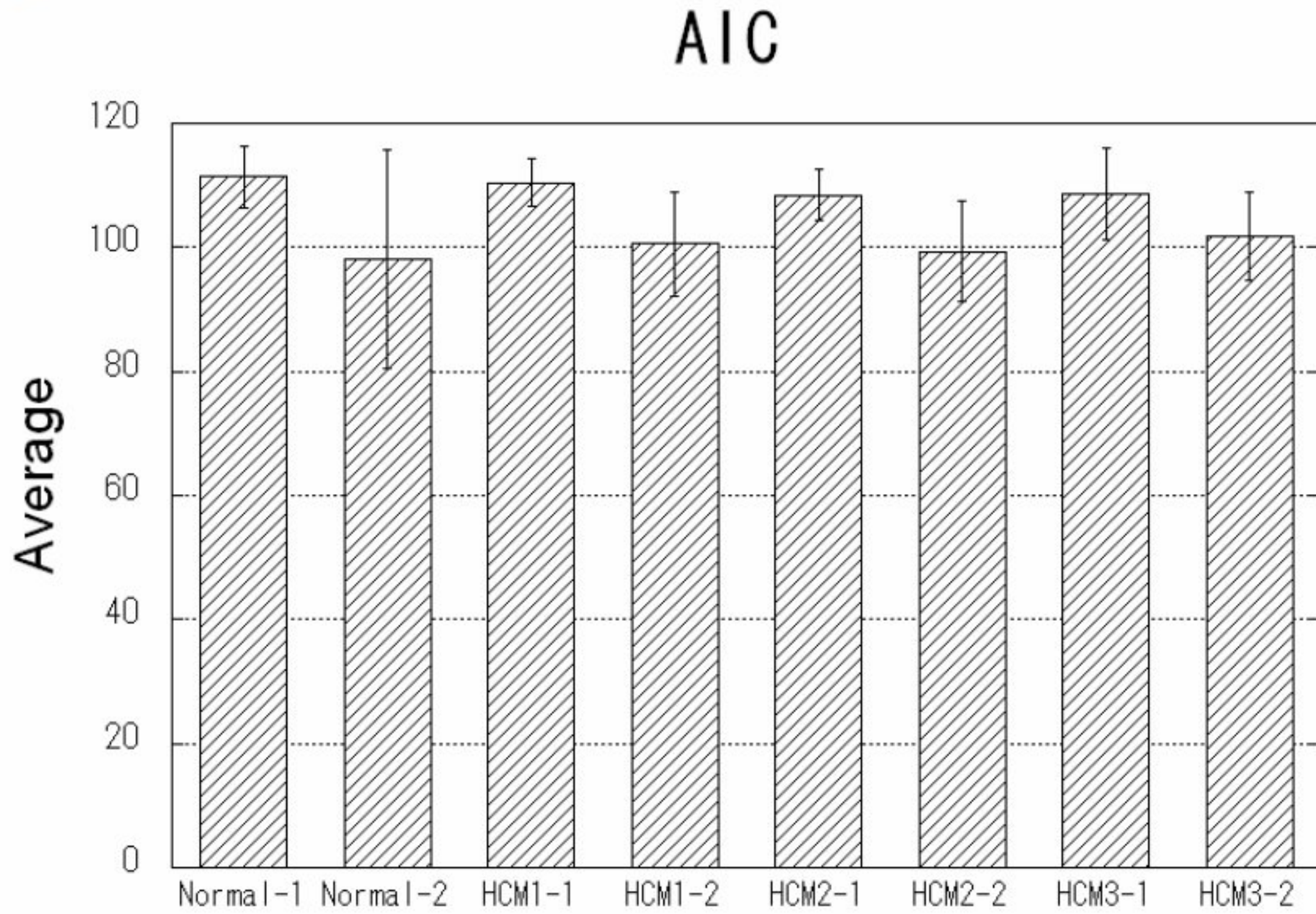


Figure 4A

(counts)

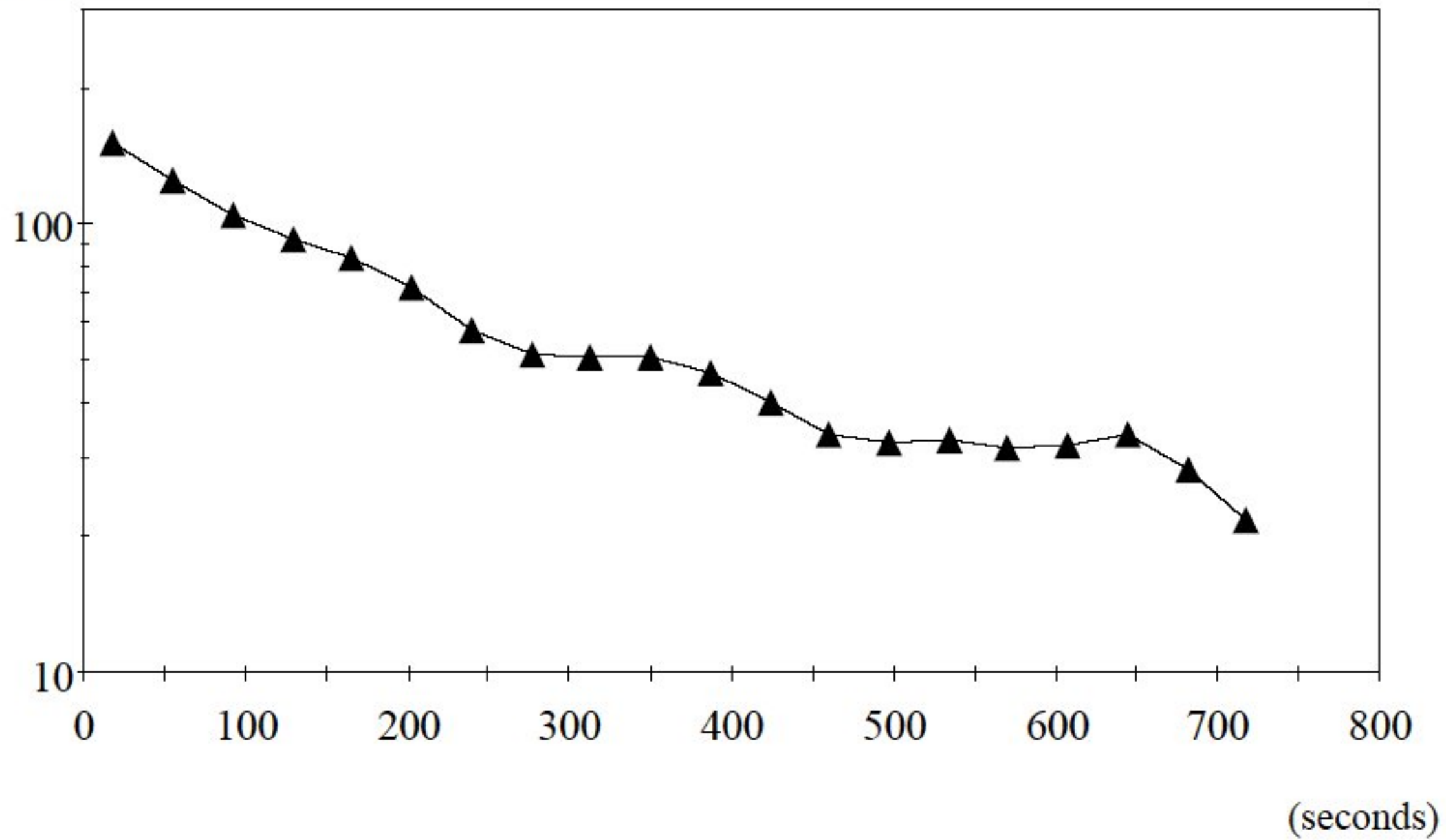


Figure 4B

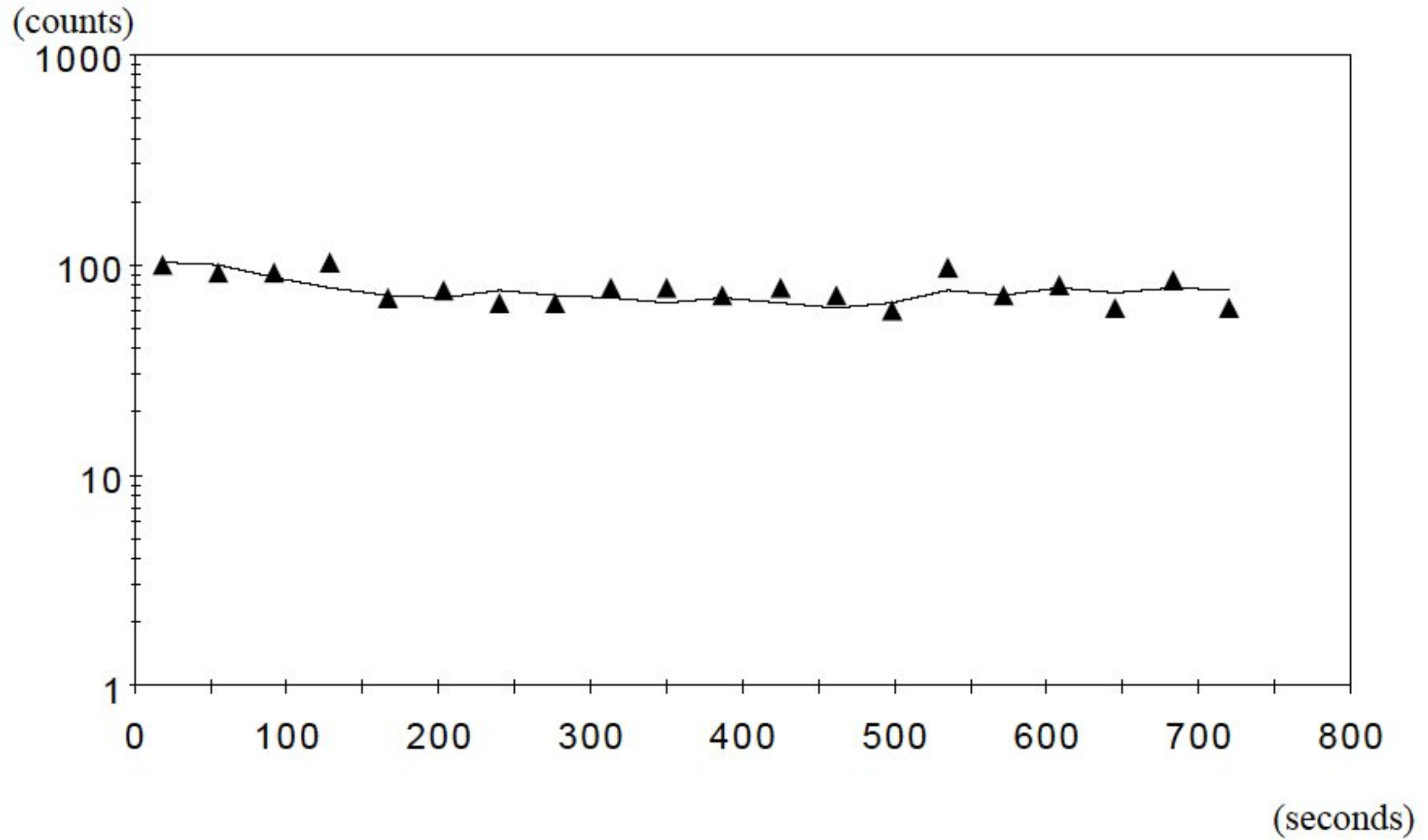


Figure 4C

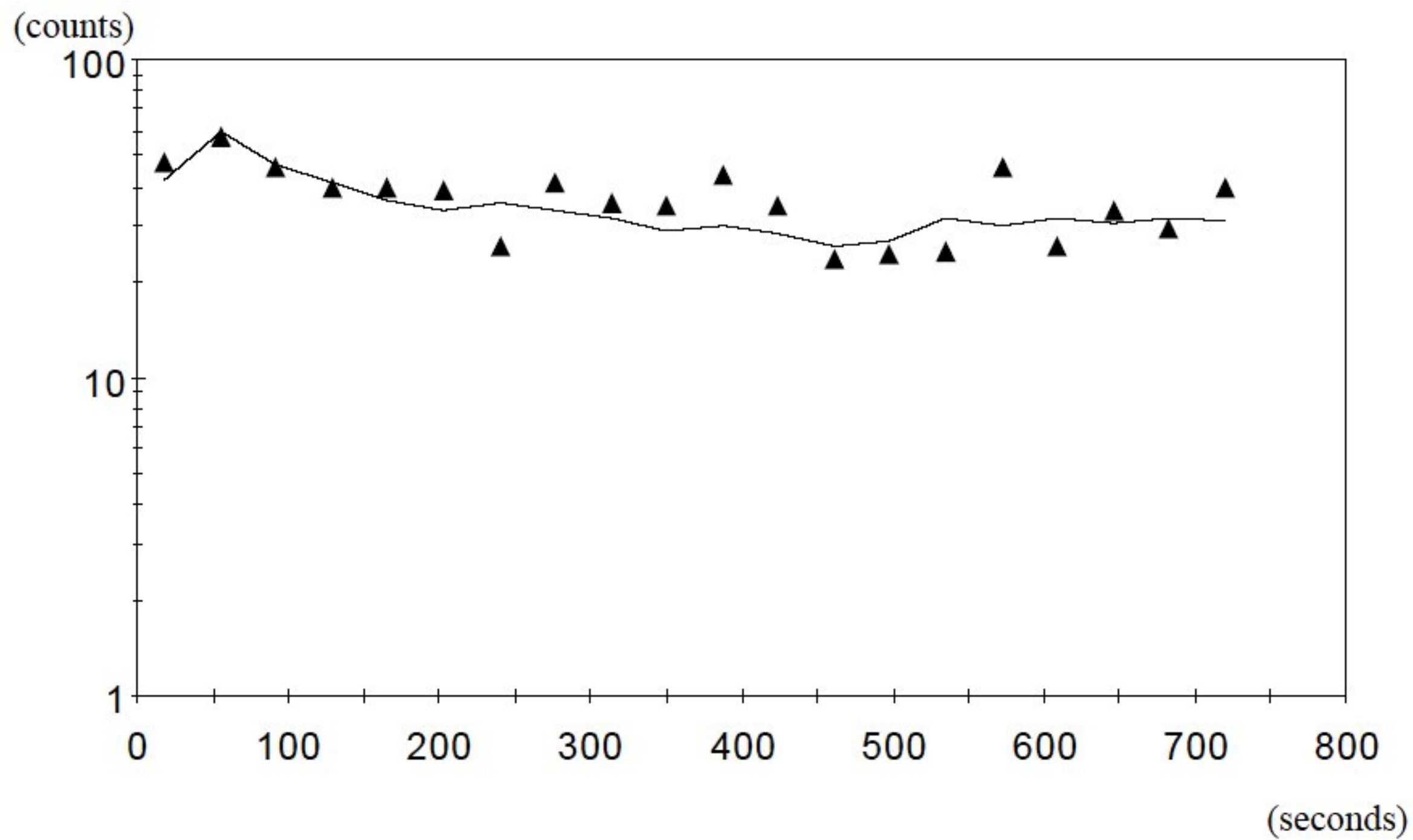


Figure 4D

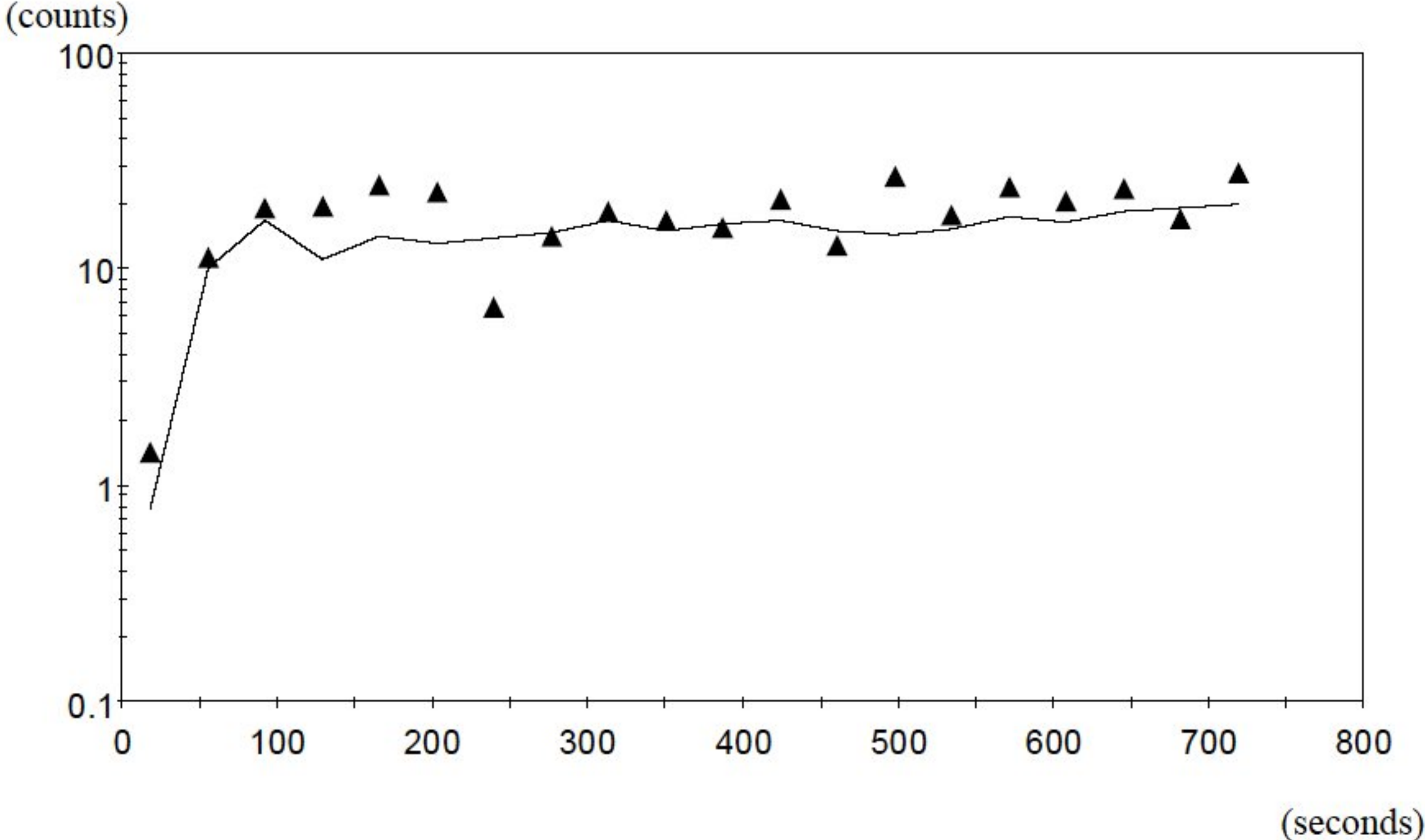


Figure 4E

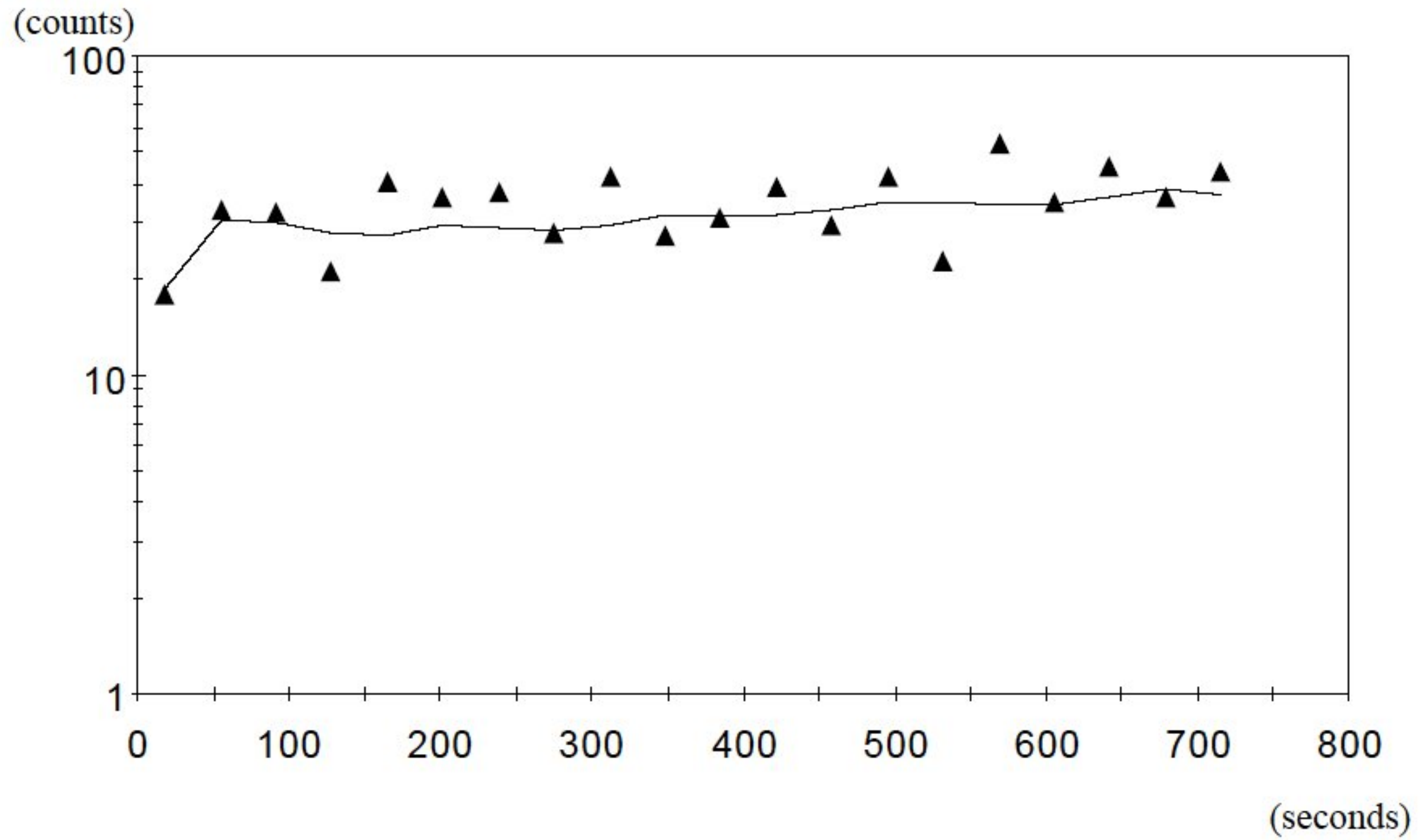
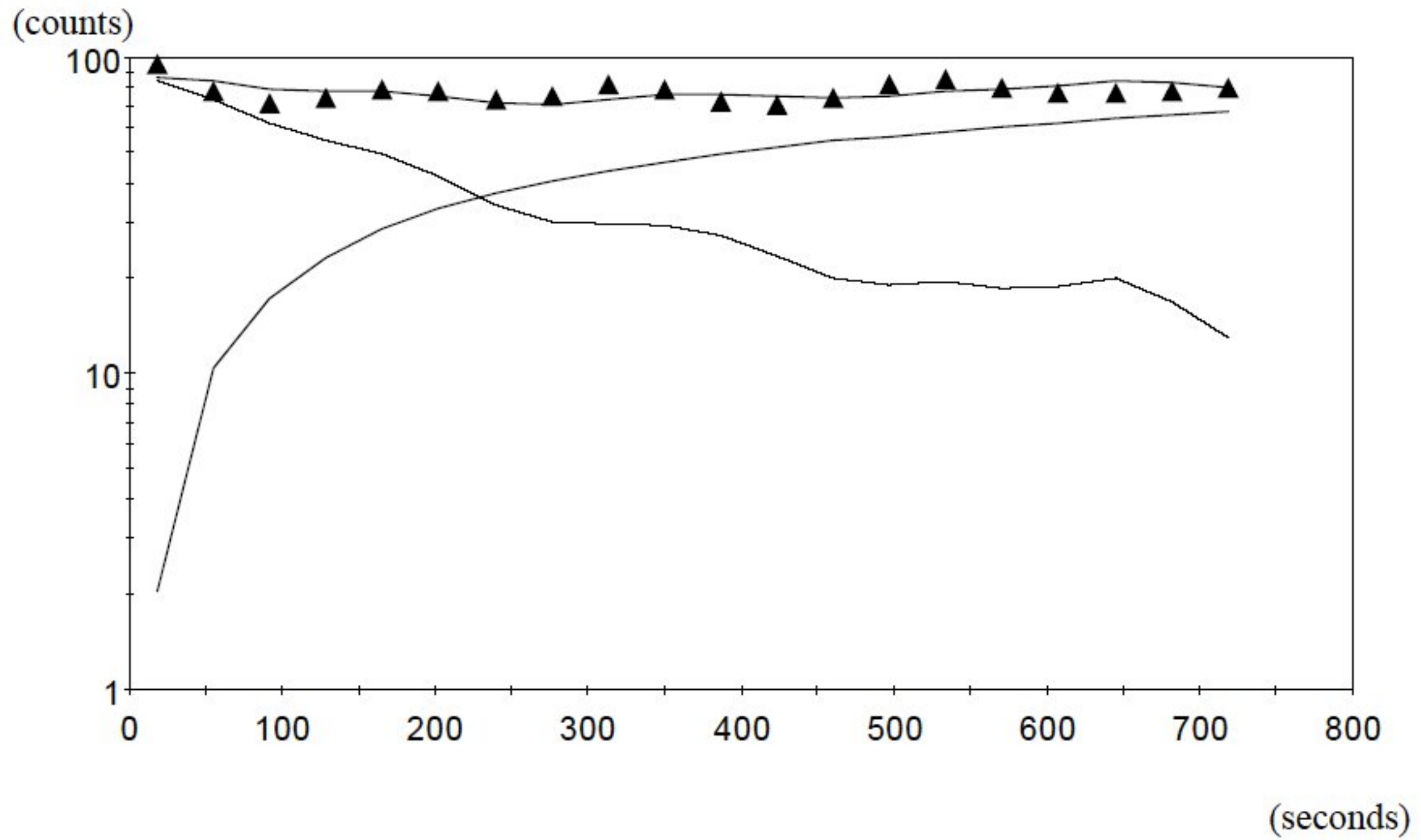


Figure 5



Legends

Figure 1

This schema shows the 1-compartment model (A) and the 2-compartment model (B). In 1-compartment mode, first compartment (C1) is reversible tissue compartment, k_1 and k_2 represent influx and outflux rate constant for the reversible tissue compartment, respectively. The 2-compartment model had second compartment (C2) in addition to the 1-compartment model. C1 is reversible tissue compartment and C2 is irreversible tissue compartment. k_1 and k_2 also represent influx and outflux rate constant for the reversible tissue compartment, and k_3 represents specific uptake rate constant for the irreversible tissue compartment, respectively.

Figure 2

This is an example of I-123 BMIPP dynamic SPECT images. Each image is mid-ventricular short-axis image of the same slice location. Assigned number is the frame number, the frame time is 30 seconds.

Figure 3

This bar graph shows the average AIC scores of 1- and 2-compartment model in normal, early, moderately advanced and severely advanced HCM ROIs. Data are reported as mean +/- standard deviation. The average AIC scores of 2-compartment model were significantly smaller than 1-compartment model in 4 groups of ROIs. Normal-1 and Normal-2 = 1- and 2- compartment model in normal ROIs; HCM1-1 and HCM1-2 = 1- and 2- compartment model in early HCM ROIs; HCM2-1 and HCM2-2 =

1- and 2- compartment model in moderately advanced HCM ROIs; HCM3-1 and HCM3-2 = 1- and 2- compartment model in severely advanced HCM ROIs, respectively.

Figure 4

This plot shows a typical input function (A) and fitting curves of a normal (B), an early HCM (C), a moderately advanced (D) and a severely advanced HCM ROI (E). The vertical axis shows the radioactivities (counts per 30 seconds) of the ROI in the center of the LA (A) or the segment (B-E), and the horizontal axis shows time from the injection.

Figure 5

This plot shows a simulation of each compartment with Win SAAM software. Triangles show observed data. A thin line represents the activity in the reversible tissue component (C1) and thick line represents in the irreversible tissue component (C2). The activity in reversible tissue component was gradually decreased and it in irreversible tissue component was increased with time until 15 minutes after the injection.

Table 1. Rate constants in each group

	k1 (FSD %)	k2 (FSD %)	k3 (FSD %)	k1/k2 (SD)	k1k3/k2 (SD)	k1k3/(k2+k3) (SD)	R
Normal	0.097 (149.2)	0.158 (169.9)	0.00306 (32.7)	0.679 (0.203)	0.00189 (0.0004)	0.00181 (0.0003)	0.89
LVH	0.112 (169.6)	0.173 (192.5)	0.00306 (34.2)	0.669 (0.196)	0.00188 (0.0004)	0.00179 (0.0004)	0.87
HCM1	0.098 (180.9)	0.183 (207.4)	0.00388*** (38.1)	0.598*** (0.258)	0.00192 (0.0005)	0.00177 (0.0004)	0.87
HCM2	0.057* (114.6)	0.111* (137.0)	0.00376*** (33.7)	0.547*** (0.176)	0.00183 (0.0004)	0.00171* (0.0004)	0.85
HCM3	0.087 (280.3)	0.208 (310.1)	0.00372* (32.6)	0.475** (0.139)	0.00163* (0.0004)	0.00153** (0.0004)	0.82

* P < 0.05; ** P < 0.005; *** P < 0.00001 compared with normal

R: Pearson product-moment correlation coefficient for fitted curves and observed data;

LVH: LVH due to eHT;

HCM1: early HCM;

HCM2: moderately advanced HCM;

HCM3: severe advanced HCM

Table 2A. Binominal logistic regression analysis

	k1	k2	k3	k1/k2	k1k3/k2	k1k3/(k2+k3)
P value	0.462	0.914	0.0005	0.966	0.0001	0.0021

Table 2B. Multinomial logistic regression analysis

	k1	k2	k3	k1/k2	k1k3/k2	k1k3/(k2+k3)
P value	0.132	0.553	0.0333	0.0063	0.695	0.803